JOURNAL OF AIRCRAFT
Vol. 43, No. 2, March–April 2006

Experimental Study on Aircraft Landing Gear Noise

Y. P. Guo* and K. J. Yamamoto†
Boeing Phantom Works, Huntington Beach, California 92647
and
R. W. Stoker‡
Boeing Phantom Works, Seattle, Washington 98124

An experimental investigation on aircraft landing gear noise is presented. The study includes systematic testing and data analysis using a full-scale Boeing 737 landing gear. The database covers a range of mean flow Mach numbers typical of landing conditions for commercial aircraft and various landing gear configurations, ranging from a fully dressed, complete gear to cleaner configurations involving only some parts of the complete gear. This enables the examination of noise radiation from various groups of the gear assembly and the derivation of functional dependencies of the radiated noise on the flow Mach number at various far-field directivity angles and on various gear geometry parameters. It is shown that the noise spectrum can be decomposed into three frequency components, namely, the low-, mid-, and high-frequency components, respectively, representing contributions from the wheels, the main struts, and the small details such as hoses, wires, cutouts, and steps. It is found that these different frequency components have different dependencies on flow parameters and gear geometry. Based on the spectral decomposition in the three frequency domains, normalized spectra are derived for all three components and a model for the overall sound levels is developed as a function of flow and geometry parameters.

Nomenclature

B_n	=	coefficients of normalized spectrum, $n = 0, 1, 2, 3, 4, 5$
C_n	=	coefficients of overall sound pressure level, $n = 0, 1, 2, 3, 4, 5$
D	=	wheel diameter
d	=	strut diameter
F	=	normalized spectrum
f	=	frequency
ℓ	=	length scale
M	=	incoming flow Mach number
N_s	=	number of struts
N_w	=	number of wheels
p	=	sound pressure
R	=	radial distance of far-field microphone
Sr	=	Strouhal number
U	=	mean flow velocity
η	=	complexity factor
θ	=	polar angle of microphone location

I. Introduction

AIRCRAFT landing gear noise has been recognized in recent years as one of the major contributors to the total aircraft noise, especially at landing conditions. Its prediction, however, remains one of the most difficult challenges in aeroacoustics because of the complexity of the gear geometry and the surrounding flowfield. Though significant progress has been made in computational power and numerical simulation methodologies in recent years, solving the unsteady flowfield around a practical landing gear assembly, and, hence, computing the noise field, is still not a practical task. This is very likely to remain so for many years to come, and our best hope to develop useful prediction tools for the foreseeable future probably lies in empirical approaches and other approximate methods. The former has of course always been followed by researchers and engineers,[1–5] whereas efforts of developing the latter have also been attempted in recent years. An example is the statistical modeling that promises to bring in more physics to the prediction.[6] In this paper, we present an experimental study on landing gear noise and the development of an empirical prediction tool. The study is based on systematic testing and data analysis of the full-scale Boeing 737 landing gear.

The difficulty in landing gear noise prediction can be attributed to the large number of components in the gear assembly, which always have very different sizes, shapes, and orientations. A precise understanding of how each of them generate noise and how they interact with each other is not practical and probably not necessary either. It is desirable and useful, however, to be able to catalog the gear components into groups according to the characteristics of their noise and to understand the relative importance of these groups in contributing to the total landing gear noise. Clearly, this helps identify the dominant noise sources and can lead to noise reduction treatments targeting the most offensive group, achieving the most effective and economic solution. It also helps the development of prediction tools, both empirical and numerical, by providing a database consisting of not only the total noise but also individual noise components for tool validation. To separate explicitly the noise contributions of different component groups, a series of gear configurations with various degree of complexity was used in our tests. This enables us to catalog the landing gear assembly into three groups, namely, the wheels, the main struts, and the small features. The last group includes all of the small parts such as brake braces, hydraulic hoses, and wires, as well as small geometry irregularities such as cutouts and steps. We choose to work with this grouping because these three groups have very different characteristic length scales and, hence, generate noise in different frequency domains. The logical choices of the length scales are, respectively, the diameter of the wheels, the average cross-sectional dimension of the main struts, and the typical size of the small features.

A lesson learned in recent years in landing gear noise study is the importance of the small details of the gear assembly in noise generation.[7–10] In early studies of landing gear noise and empirical tool development, small-scale and, thus, inevitably simplified

Received 24 May 2004; revision received 15 September 2004; accepted for publication 2 October 2004.

*Boeing Technical Fellow, Mail Code H013 B308, Department of Acoustic Technology. Associate Fellow AIAA.
†Senior Engineer, Mail Code H013 B308, Department of Acoustic Technology. Member AIAA.
‡Senior Engineer, Mail Code 67ML, Department of Noise Engineering. Member AIAA.

models were used to generate the database.[1–3] It is now known that tools developed from such databases are grossly in error, missing the significant high-frequency noise component that dominates the calculations of noise metrics such as the effective perceived noise levels (EPNL). This is essentially because the small-scale simplified models cannot include the small details of real landing gears. By cataloging the gear components and separating their respective noise contributions, we can explicitly show the dominance of the small details in generating high-frequency noise. By comparing the test data with predictions based on existing models derived from earlier studies, we will show that predictions without the contributions from small parts in the landing gear greatly underpredict test data in the high-frequency domain, leading to a prediction in EPNL about 8 dB lower than the test data. This immediately leads to two conclusions. One is that potential effective noise reduction treatments may have to target the small parts in the landing gear, by smoothing out steps and filling in cutouts, for example. The other conclusion is that prediction tool development must include the capability of high-frequency noise prediction. Because this makes the tool development much more difficult, it is sometimes easily overlooked. Early experimental studies missed it, and some recent numerical simulations are also limited to the large parts such as wheels and struts.[11–13] These may be considered as a sensible starting point to develop numerical methodologies and expertise, but are far from being useful in practical landing gear noise prediction.

In low Mach number flows with rigid bodies, the noise is often scaled on the flow Mach number by the sixth power law.[14–16] We will show that this indeed describes the low- and mid-frequency noise, but the spectra of the high-frequency noise is better scaled by the seventh power law (corresponding to an eighth power law for the sound intensity or overall sound level), which is typical of noise generated by turbulent flows themselves, instead of the unsteady forces on the surfaces of the bodies in the flow.[17] Furthermore, we find that the high-frequency landing gear noise has spectral shapes that fall off approximately in proportion to the inverse square of frequency, again, typical of turbulence generated noise. This may seem to contradict the commonly known sixth power law that attributes the noise sources to the unsteady forces on the bodies and, hence, in analogy to dipole sources. It is, however, readily explainable once it is recognized that high-frequency noise sources are not likely to be compact, an assumption implied by the sixth power scaling law in aeroacoustic theories. At low and mid frequencies, the acoustic wavelength is relatively large compared with the typical dimension of the bodies with which the flow interacts. Thus, the bodies can be regarded as acoustically compact, complying with the dipole radiation analogy. At high frequencies when the acoustic wavelength is comparable to and/or smaller than the body dimensions, the bodies become acoustically noncompact. The dipole sources due to the surface pressure fluctuations become a distribution with rapid phase variations. The noise radiation from such a dipole source distribution suffers severe mutual cancellation between the source elements, significantly reducing the radiation efficiency. As a result, the effects of the bodies are mainly to reflect the noise from the sources in the flow, acting as sounding boards.[18] Thus, the radiation at high frequencies is essentially from the turbulent flow surrounding the landing gear, governed by the eighth power law. We will show that this physical reasoning is consistent with measurements from the phased microphone array that identifies the high-frequency sources to be a distribution in the wake of the gear.

For each of the three frequency domains, empirical formulas will be derived for the sound pressure as a function of the flow conditions, gear geometry, and microphone locations. The implementation of such empirical prediction is straightforward. When the Mach number dependence is applied, however, note that the Mach number should be the local flow Mach number just upstream of the landing gear, which can be noticeably different from the mean flow Mach number of the freestream far away from the aircraft. We will show that due to the installation effects of the wing, the local flow Mach number just upstream of a main landing gear can be 20% smaller than the freestream flow Mach number. This corresponds to a difference in noise of as much as 5.8 dB according to the sixth power law. Similarly, the local flow velocity just upstream of a nose gear can be noticeably higher than the freestream flow velocity because of the flow acceleration when passing the nose of the fuselage. This increase of flow velocity will lead to an increase in landing gear noise, which needs to be accounted for when predicting landing gear noise for airplanes.

The empirical prediction for each frequency domain correlates the noise not only to parameters such as flow Mach number and far-field location, but also to geometry details such as the number of wheels and struts. For the high-frequency component that is generated by the small details of the landing gear assembly, namely, the hoses, wires, cutouts, and steps, it is clearly not practical to have a precise description of the small features, because of their irregular shapes, sizes, and locations, nor is it necessary to define them precisely for noise prediction that is also affected by many other things. Instead, we will introduce a complexity factor to characterize the aggregate effects of the small features and empirically relate the high-frequency noise to this complexity factor. Intuitively, the larger the aircraft is, the more complex the landing gear needs to be. Thus, the complexity factor can be related to aircraft gross parameters such as the maximum takeoff (or landing) weight. Though this is obviously not a unique definition to account for the high-frequency landing gear noise generation, it does provide a practical approach for commercial airplane noise prediction.

II. Test Facility and Data Acquisition

The test was conducted in Boeing's Low Speed Aeroacoustic Facility (LSAF), the general layout of which is shown schematically in Fig. 1. The facility includes a 9 by 12 ft freejet in a large anechoic test chamber. The chamber measures 65 ft long, 75 ft wide, and 30 ft high. The chamber with the existing foam wedges allows for broadband measurements between 200 Hz and 80 kHz. The flow supply is through two centrifugal fans operating in parallel, each having a 107-in. wheel with backward inclined airfoil blades and powered by a 5200-hp synchronous motor. Tunnel speed is controlled by variable-frequency motor speed controls operating remotely from the LSAF control room, over a range of Mach numbers $M = 0.05$–0.25. The freejet exhaust is through a 19 by 19 ft exhaust collector. To cover typical landing conditions for commercial airplanes, for which landing gear noise is of concern, a range of wind tunnel Mach numbers were tested, from 0.18 to 0.24 with an increment of 0.02. The landing gear was mounted from the overhead strut in the facility. A splitter plate was also attached to the overhead strut to simulate a wing underbody. A cavity was built into the splitter plate to examine the effect of the wing cavity on the radiated noise. No wheel well cavity was built or simulated. A photograph of the test chamber with the Boeing 737 landing gear installed is shown in Fig. 2.

Two types of acoustic measurements were made during the test, one by a phased microphone array and the other by free far-field microphones. The measurement equipment locations are shown schematically in Fig. 3. The far field microphones were mounted on poles attached to the test chamber floor. There were 12 pole-mounted

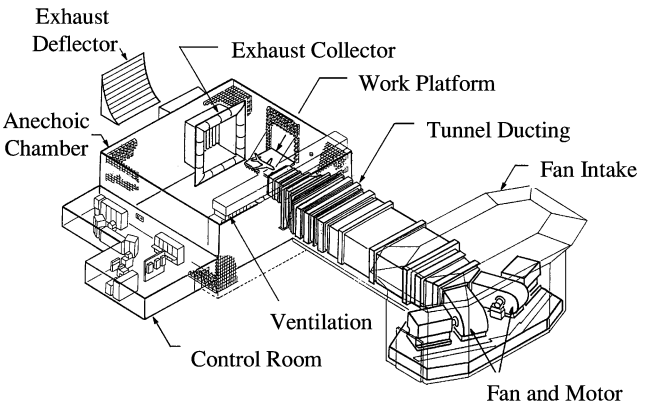

Fig. 1 Schematic of Boeing LSAF used for landing gear noise test.

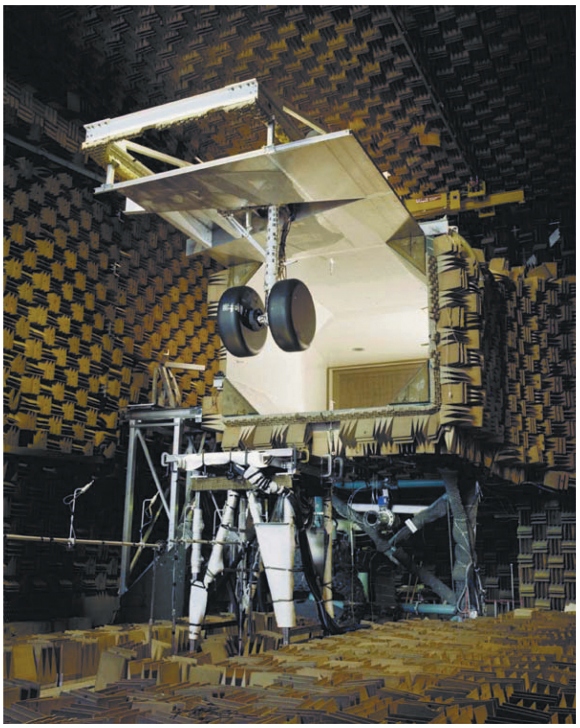

Fig. 2 Boeing 737 landing gear installed in LSAF for noise test.

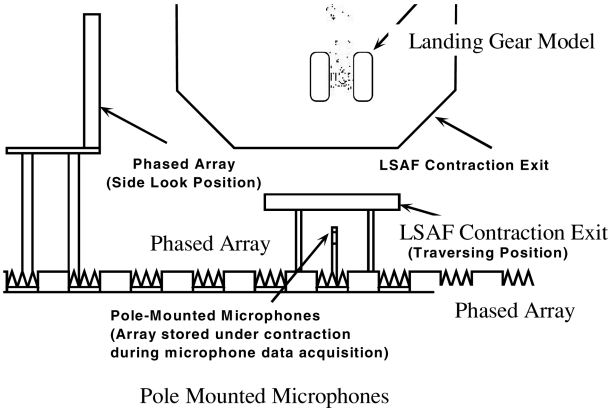

Fig. 3 Setup for landing gear noise test in Boeing LSAF.

microphones placed along the simulated flight path at 60, 65, 70, 75, 80, 90, 100, 110, 120, 130, 140, and 150 deg with the 90-deg position being directly below the gear assembly. This is a range in which landing gear noise is most likely to have significant contributions to the total aircraft noise. Outside of this range, fan inlet noise dominates at small angles and aft fan and jet noise dominate at large angles. Sound levels in one-third octave bands from 50 Hz to 30 kHz were measured with the microphones. The microphones were 1/4-in. Bruel and Kjaer 4135 type and were mounted 117 in. below the wind tunnel centerline, simulating the flight path. In addition to the far-field free microphones, a phased microphone array was also used in the test. The microphones in the array were nested in an area approximately 8 ft in diameter. The array design consisted of two nests, a small high-frequency array and a large low-frequency array. The small high-frequency array was nested within the large low-frequency array, and the two arrays shared some microphones. The array was mounted either to the side of the landing gear or below it in the fly-over position (Fig. 3). For both mounting positions, the array was traversed over the angular range from 60 to 120 deg to resolve the directivity of the noise field. The position below the gear is clearly of interest to fly-over noise, but the side-view position was used to resolve source locations more clearly. The measured flow

Fig. 4 Full-scale Boeing 737 main landing gear.

and ambient quantities include tunnel freestream Mach number, ambient temperature in the test arena, ambient/barometric pressure in the test arena, freestream total pressure, relative humidity in the test arena, and freestream velocity.

The objective of the test is to evaluate the noise from a full-scale landing gear with particular emphasis on the effects of geometry details on the far-field noise spectrum and the relative noise contributions of the components in the gear assembly. To this end, the test used a full-scale Boeing 737 landing gear, which is typical of most Boeing landing gears. It has a main strut structure, a drag brace system, a side brace, multiple hydraulic lines, and brakes. A photograph of this landing gear is shown in Fig. 4. The main difference between the Boeing 737 main landing gear and those for other Boeing airplanes is the number of wheels; the Boeing 737 has two wheels, whereas the other airplanes have either four or six wheel trucks on the main landing gear. For the purpose of examining the noise generated by small details on the landing gear, the Boeing 737 model is considered sufficient because it is typical of most Boeing landing gears in small details.

To reveal the noise contributions from different parts of the landing gear, six variations of the landing gear configurations were tested. In addition to the fully dressed (dirty) configuration with all the small details such as hydraulic hoses and electric wires as shown in the photograph in Fig. 4, a clean configuration was tested that lacked the brake assembly and other dressing items. This clean configuration gear is shown in the photograph in Fig. 5 together with two closeup comparisons with the dirty configuration. To derive the contributions from the wheels, a further simplified configuration was tested, similar to the clean configuration, but with the wheels removed and with only the main connecting struts remaining. Also, wheels of different sizes were tested. Furthermore, to see how the number of wheels is correlated to the amount of radiated noise and to examine the wheel-to-wheel interactions, a six-wheel truck was built and tested. The six-wheel truck consisted of two wheels attached in front and two wheels attached aft of the center wheels. However, no small details such as brakes and wires were added to the additional wheel trucks so that the six-wheel truck is considered a partially dressed landing gear. The test configurations were designed in this way such that three groups of gear components are easily cataloged. These are the wheels, the main struts, and the small features. To facilitate discussions, all six configurations are summarized in Table 1, and their definitions are given in Table 2 to show what groups of gear components each of them contain. Table 2

Table 1 Test configurations and descriptions

Configuration	Description
A	Fully dressed with two large wheels
B	Clean with two large wheels
C	Clean without wheels
D	Fully dressed with two small wheels
E	Clean with two small wheels
F	Partially dressed with six wheels

Table 2 Definitions of configurations and their corresponding frequency domains

	Components			Frequency		
Configuration	Wheels	Struts	Details	Low	Mid	High
A	✓	✓	✓	✓	✓	✓
B	✓	✓		✓	✓	
C		✓			✓	
D	✓	✓	✓	✓	✓	✓
E	✓	✓		✓	✓	
F	✓	✓	✓	✓	✓	✓

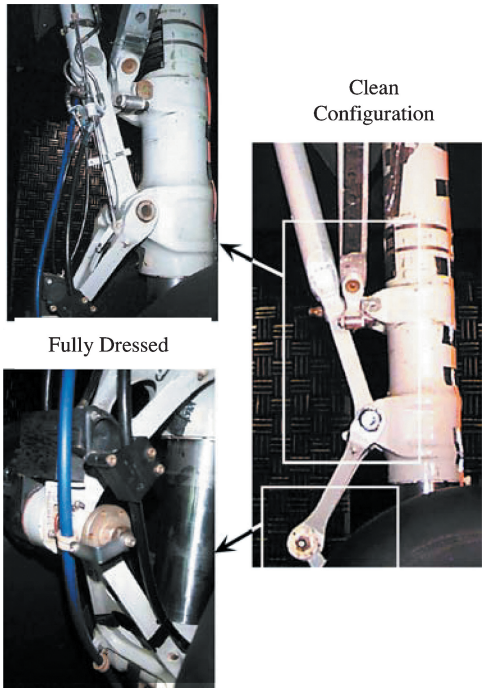

Fig. 5 Dirty and clean configuration comparison of Boeing 737 landing gear.

also lists the frequency domains that the various configurations are expected to cover. For example, configuration C is defined in Table 1 to be a clean gear without wheels. Thus, it only contains the main struts and is expected to radiate noise in the mid-frequency domain as indicated in Table 2.

III. Data Analysis

The test data were acquired and processed automatically with the output in terms of one-third octave band sound pressure level (SPL). In the data analysis presented here, some standard corrections have been applied to comply with conventionally acceptable format. First, because the test facility is a freejet wind tunnel and the microphones are outside the flow, shear layer corrections were applied to all of the measurements according to the method described in Ref. 19. Because the microphones are located along a line below the gear with different distances to the gear center, the sound waves experienced different amounts of atmospheric absorption when they propagate from the landing gear to the microphones. In the data analysis, the

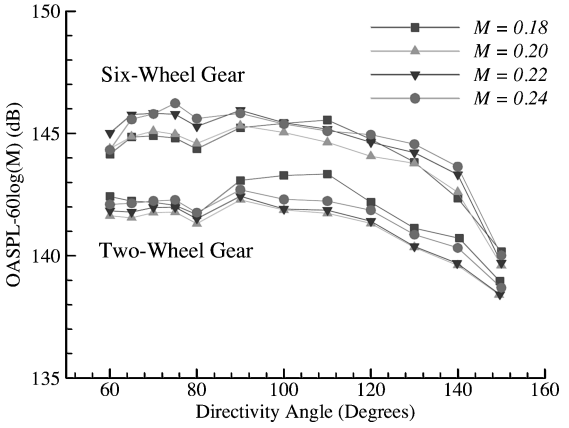

Fig. 6 OASPL as function of microphone angles for two gear configurations at various Mach numbers.

atmospheric absorption is taken out of the data so that the results become lossless. In the test setup, the microphones are not very far away from the gear. (The overhead microphone is about 10 feet from the gear center.) Thus, the atmospheric absorption correction is small. Note that, because the sources are not at a single point, the absorption correction can only be done empirically by assuming a source location at the gear center. The cutoff frequency of the LASF anechoic chamber is about 200 Hz. In the data analysis, frequencies below 200 Hz were discarded when computing the overall sound pressure level (OASPL), which is the integration of SPL over frequency. However, in the empirical prediction scheme, these low frequencies are recovered by extrapolation.

With the data reduced to standard format, parametric trends can be analyzed. The flow conditions are mainly characterized by the flow Mach number. As is well known in aeroacoustics, noise generation in unsteady low Mach number flows in the presence of rigid, smooth bodies usually follows the sixth power law. With the use of this scaling, the normalized OASPL is shown in Fig. 6 as a function of the microphone angles for two sets of data, one for the fully dressed gear (configuration A) with two wheels and the other for the partially dressed six-wheel configuration (configuration F). The results show satisfactory collapsing with variations of about 1 dB (except for the case of $M = 0.18$ for the fully configured two-wheel gear, which will be explained in detail later in this section). The sixth power law can also be used to scale the sound pressure spectra. Some examples are given in Fig. 7 for the fully dressed configuration at three microphone angles. The data seem to follow the sixth power scaling well, especially for low frequencies, again with the exception of the case of $M = 0.18$ at approximately 800 Hz, to be explained later. At high frequencies, the deviation from the sixth power law becomes noticeable, with lower Mach number data having lower noise levels. This means the high-frequency noise should be scaled on a higher power law. To demonstrate this clearly, Fig. 8 shows the SPL for the fully configured gear at the overhead location, with both the sixth power and the seventh power scaling. The seventh power scaling works apparently better for high frequencies, whereas the sixth power scaling collapse the data very well in the low- and mid-frequency domain. The transition from the sixth to the eighth power is of course continuous in frequency, as seen in Fig. 7 with the gradual increase of the deviation from the sixth power law as frequency increases. Note that because the one-third octave SPL is computed by integrating the narrowband results with fixed-frequency range for all cases of different Mach number, the seventh power scaling for SPL corresponds to an eighth power law for the OASPL or sound intensity, which is the well-known scaling for noise generated by turbulent flows.

At first glance, this seems to contradict the well-known result of noise radiation from unsteady forces on rigid bodies, which scales on the sixth power. In fact, it is readily explainable by the principles of aeroacoustics. As is well known, the sixth power law is applicable to bodies of compact dimension, in comparison with

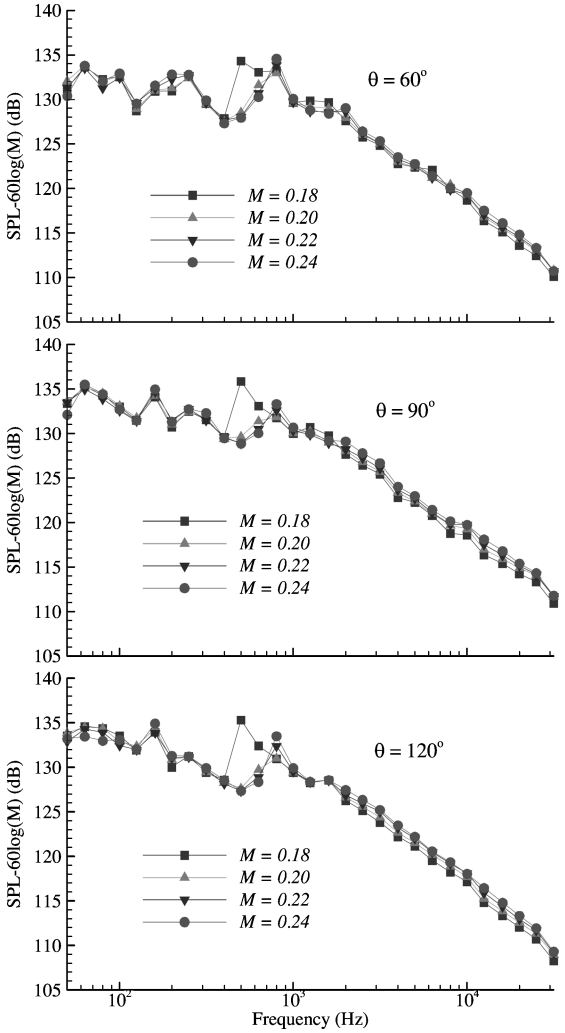

Fig. 7 Normalized SPL as a function of frequency for fully configured gear configuration at three microphone angles.

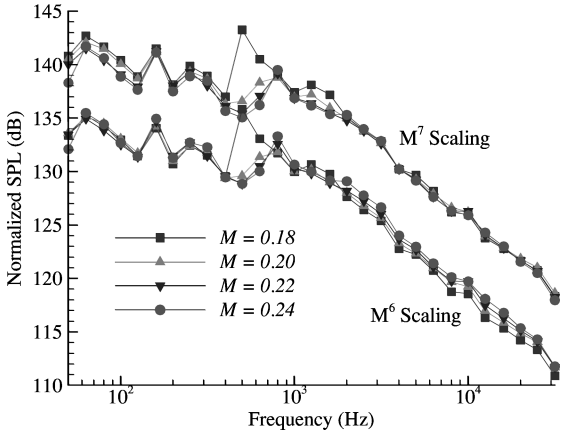

Fig. 8 Different Mach number scaling comparison on the SPL for fully dressed gear configuration at overhead position.

the acoustic wavelength. Thus, the scaling is followed well at low frequencies where the acoustic wavelength is large, making the bodies acoustically compact. In this case, the radiation is due to the dipoles furnished by the unsteady forces on the body surfaces. At high frequencies with short acoustic wavelength, the bodies become non-compact in relation to the wavelength. The surface pressures have significant phase variations within a wavelength so that their radiation suffers severe mutual cancellation. As a result, the dipole radiation degrades to quadrupole radiation and the bodies essentially reflect/diffract the noise from the unsteady flow, which scales on the eighth power law. The body surfaces are only sounding boards that do not alter the radiation efficiency of the unsteady flow. The almost perfect data collapsing shown in Fig. 8 with the seventh power law for the high-frequency noise is precisely due to this physical mechanism.

Again, note that the seventh power scaling for the SPL corresponds to an eighth power law for the OASPL or sound intensity because the one-third octave SPL is for fixed-frequency band, not fixed-Strouhal number band. The low- and mid-frequency spectra in Figs. 7 and 8 have the same Mach number scaling (the sixth power law) as the OASPL because the spectra at these frequencies have a broad maximum. The integration to obtain the OASPL is independent of whether fixed-frequency band or fixed-Strouhal number band is used for the low- and mid-frequency components. It makes a difference for the high-frequency component because the spectra at high frequencies have a falloff slope. The collapsed data in Fig. 8 show a high frequency falloff approximately proportional to an inverse power law in frequency to the power of 1.2. The results are in one-third octave band, implying that the corresponding narrowband spectra have a high frequency falloff approximately proportional to the inverse square of frequency. Again, this is a typical spectral feature of noise generated by turbulent flows.

When the phased microphone array measurements are analyzed, the source distribution around the landing gear can be revealed. The identification of the source locations can then shed light on the nature of the sources, whether they are the unsteady forces on the landing gear components or the unsteady flow in the wake, for example. The phased array was used in two positions in the test, one below the gear and the other on the side. The position below the gear simulates the fly-over position and is relevant to aircraft noise. However, it has limited resolution both because of the relatively small distance between the array and the gear and because of the blocking effects of the wheels. The wheels reflect/diffract the sound waves from sources associated with the struts and other gear components that are located above the wheel truck before they reach the microphone array. This can mask the true location of the sources, making the source identification unreliable. To illustrate this, some examples are given in Figs. 9 and 10 for the array at the overhead location. The results are for the fully configured gear at the Mach number of 0.2, but the results are typical of other Mach numbers. Figure 9 shows the source strength measured by the large nest of the array and, hence, for low and mid frequencies, and Fig. 10 is from the small nest array designed for high frequencies. Figures 9 and 10 have all been normalized by the maximum values of the SPL so that each part represents the relative strength of the source distribution at each frequency. At low frequencies, the acoustic wavelength is

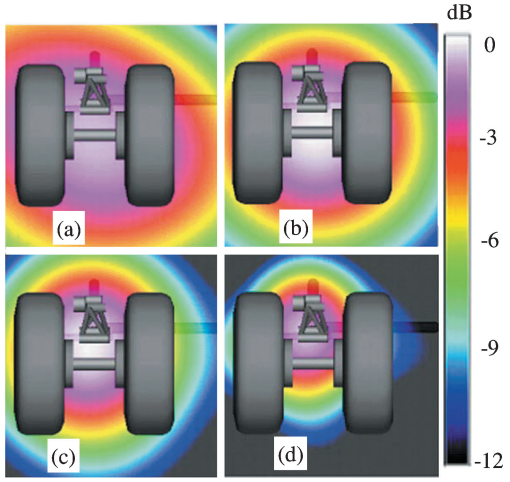

Fig. 9 Phased array measurements from overhead position for low and mid frequencies: a) $f = 225$ Hz, b) $f = 475$ Hz, c) $f = 600$ Hz, and d) $f = 850$ Hz.

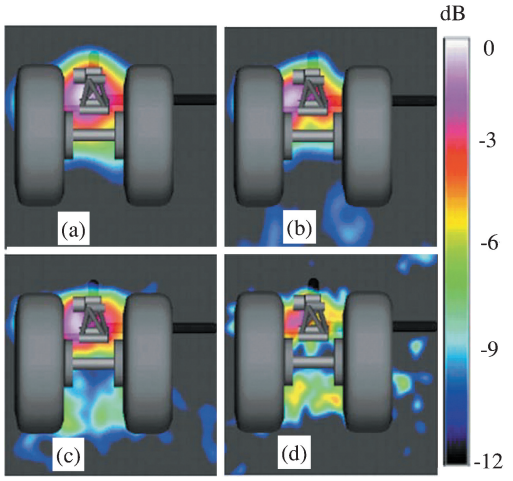

Fig. 10 Phased array measurements from overhead position for high frequencies: a) $f = 4000$ Hz, b) $f = 6000$ Hz, c) $f = 8000$ Hz, and d) $f = 10{,}000$ Hz.

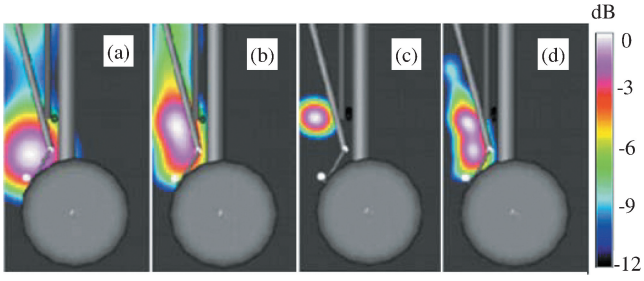

Fig. 11 Phased array measurements from side-view position for low and mid frequencies: a) $f = 1000$ Hz, peak SPL = 94.8 dB; b) $f = 1500$ Hz, peak SPL = 88.9 dB; c) $f = 2000$ Hz, peak SPL = 96.0 dB; and d) $f = 2500$ Hz, peak SPL = 83.0 dB.

long, which limits the resolution of the measurements. That is why the low and mid frequency in Figs. 9 basically show all of the noise sources as a single one, covering almost the entire gear assembly. The array position below the gear also makes the identification of the individual sources difficult, especially those behind the wheels. At high frequencies, the array resolution becomes better so that some sources are identified at the location of the torque link, as shown in Fig. 10. It can also be seen from Fig. 10 that, as frequency increases, the sources become more distributed, not only seen at obvious locations such as the torque link, but also being noticeable in the wake region where there are no gear components. This clearly indicates that the wake flow is also the noise source. For example, in Figs. 10c and 10d for 8000 and 10,000 Hz, the source at the torque link location is still the strongest, but sources are seen even at locations upstream of the torque link between the two wheels. The blocking effects of the wheels, however, are still present, which makes it difficult to have clear source identification.

This is in fact the main reason for an array position on the side of the landing gear, even though airframe noise is clearly not a concern at sideline locations for the purpose of aircraft noise certification. A side-view array is exposed to the direct propagation paths of the noise from essentially all of the sources and, hence, enables a clear source identification. It can be argued that a source radiating sideways may not necessarily contribute to the overhead location below the gear. Thus, the sources identified by the array on the side-view position may have limited practical relevance. This can be expected to be true for highly directional clean sources.

For practical landing gears, the source distribution is very complex, probably involving very irregular source types and orientations. In this case, the directivity of the radiated noise is not sharply directional and the source strength distribution detected by the side-view array can provide useful information to understand the sources.

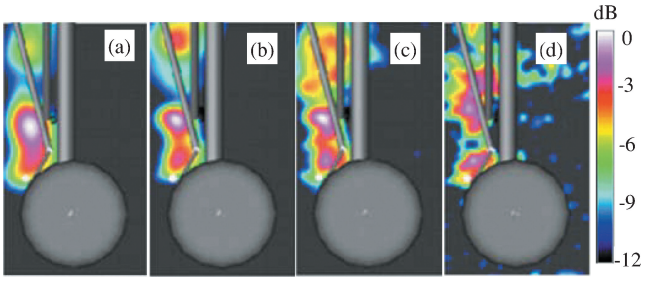

Fig. 12 Phased array measurements from side-view position for high frequencies: a) $f = 4000$ Hz, peak SPL = 78.9 dB; b) $f = 6000$ Hz, peak SPL = 72.0 dB; c) $f = 8000$ Hz, peak SPL = 64.9 dB; and d) $f = 10{,}000$ Hz, peak SPL = 59.6 dB.

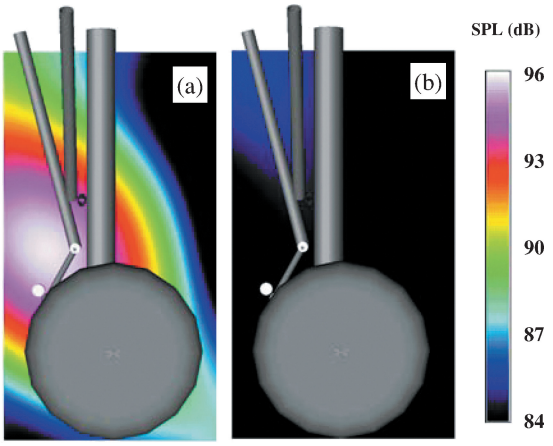

Fig. 13 Source strength comparison at 875 Hz: a) fully configured gear and b) gear with hydraulic hoses removed.

Figures 11 and 12 give such an example for the large nest array for low and mid frequencies and for the small nest array for high frequencies, respectively, both from the side-view array. Figure 11 shows that, at low and mid frequencies, the sources are localized with well-defined locations. Figures 11a–11d show that the source are located either at the torque link location or at the brake brace location or both. These are the locations with the hoses and small attachments, shown in the two closeup photographs in Fig. 5. Note that in the array source strength map shown in Fig. 11 these small components are not drawn so that the source locations do not seem to coincide with any gear parts. When Fig. 11 is compared with Fig. 5, it is clear that the source locations behind the torque link are exactly where the hydraulic hoses and the brake braces are. As frequency increases, though these two locations are still seen as strong source locations, the noise sources become more distributed, as shown in Fig. 12. Together with the results shown in Fig. 10, it is easy to see that the source distribution covers almost the entire wake, consistent with the noise spectrum measured by the free microphones, as analyzed in Fig. 8 for the Mach number scaling. Note that Fig. 12 is from the high-frequency array, which ensures that the results are not due to phased array artifact.

As mentioned earlier in this section and seen in Figs. 6–8, the case of $M = 0.18$ seems to have a particular feature. In Fig. 6, this is the case that does not seem to scale on the sixth power law with the flow Mach number. In Figs. 7 and 8, a distinctive spectral hump at about 800 Hz can be seen, which again does not seem to follow the scaling laws. The cause of this spectral hump can be identified by the phased microphone array measurements, as shown in Fig. 13. These are the results from the array location on the side of the landing gear at 875 Hz. Figure 13a shows the results for the fully dressed gear, and Fig. 13b is for the case where the hydraulic hoses and the small attachments associated with hoses in front of the torque link are removed. Clearly, the source of the tone at about 800 Hz appears to be due to the hydraulic hoses (which are readily visible in Fig. 5). The strong source location identified in Fig. 13a is where these hoses

Table 3 Combinations of various gear configurations and their effects

Operation	Effect
A − B	High-frequency noise from details
C	Mid-frequency noise from struts
B − C	Low-frequency noise from wheels
A − D	Wheel size effect
F − A	Wheel number effect
D − E	High-frequency noise from details
B − E	Wheel size effect

are. When the hoses and attachment points are removed, the noise is significantly reduced, as shown in Fig. 13b. The generation of these tones is typical of vortex shedding from bluff bodies in low Mach number flows. The frequencies of the tones increases with flow Mach number, as can be seen from Fig. 7, where the peak at 800 Hz for the $M = 0.18$ case appears to shift to 1000 Hz as the Mach number increases. Note that this figure is for one-third octave band so that the peak frequency appears to jump from one band to another. In narrow band, the tone frequency increases continuously with flow Mach number and can be estimated by equating the Strouhal number to 0.2. With the use of the hose diameters as the length parameter in the Strouhal number, the shedding frequency prediction is within 10% of the frequency shown in the data.

Testing the configurations defined in Table 1 is a convenient way to derive functional dependencies of the gear noise on various parameters and to decompose the total landing gear noise into different spectral components. The spectral decomposition is feasible because the three groups of gear parts, namely, the wheels, the main struts, and the small details, have distinctively different lengths. For the Boeing 737 landing gear, for example, the wheel diameter is about 50 in. The typical cross-sectional dimension of the main struts, is about 5 in., and the typical size of the small parts is on the order of 0.5 in. The typical lengths for the three component groups differ by decades, which, from the Strouhal number argument, would lead to frequency domains separated by decades. If the wheels generate noise mainly in the range close to 50 Hz, the main struts would generate noise around 500 Hz and the small features around 5000 Hz. All three groups of course generate broadband noise, both because of the high Reynolds number of the flow and because of the complex geometry of the gear assembly. Thus, the frequency domains have some overlapping.

To show how the noise components in different frequency domains and for different flow and geometry parameters are derived, Table 3 summarizes the operations in the data analysis that can lead to various trends. The letters in the first column are the configurations defined in Tables 1 and 2. Take the operation F minus A for example, which is the difference between the partially dressed six-wheel gear and the fully dressed two-wheel gear. The six-wheel gear is designed by simply adding two sets of two-wheel trucks to the fully dressed two-wheel gear. The additional gear trucks do not have any of the small parts, which is why configuration F is named partially dressed. Thus, the difference between F and A would be purely the effects of the number of wheels. Because wheels generate noise mainly in the low-frequency domain, the difference in noise between these two configurations can be expected mainly in low frequencies. This is indeed the case, as shown in Fig. 14, which plots the SPL for the overhead location ($\theta = 90$ deg) for the two configurations. As expected, the difference between the two configurations is significant only for frequencies below about 800 Hz. At very low frequencies below about 200 Hz, the data are contaminated by the reverberation effects of the anechoic chamber of the test facility, which manifests itself in the form of spectral humps and valleys. To help reveal the trends, two lines are shown in Fig. 14, representing the average (and probably the true data without the contamination) of the spectra. Note that the difference shown in Fig. 14 is somewhere between 4 and 5 dB. The comparison here is between two wheels and six wheels. On the basis of energy addition, the ratio 6/2 would give a noise difference of 4.8 dB. Thus, it appears that the effects of the number of wheels can be simply taking care of by the

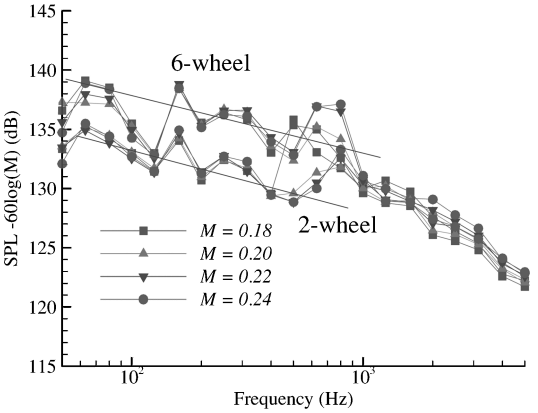

Fig. 14 Effects of number of wheels on far-field low-frequency noise at overhead position.

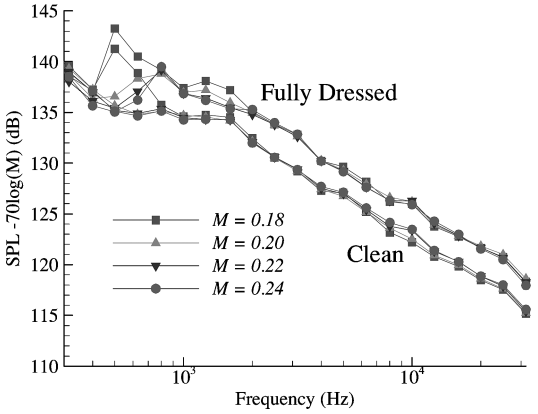

Fig. 15 Effects of small parts in gear assembly on far-field high-frequency noise at overhead position.

energy addition; doubling the number of wheels simply adds 3 dB to the noise in the low-frequency domain.

Similarly, when the difference between configuration A and B is taken, the noise from the small features in the landing gear assembly can be derived. To illustrate this, Fig. 15 shows the SPL for these two configurations for the overhead microphone position. The results are normalized by the seventh power law on flow Mach number because the high-frequency noise is expected to show most of the differences. As shown in Fig. 15, the high-frequency noise has an almost uniform increase from the clean configuration to the fully dressed configuration for frequencies above about 800 Hz. This clearly demonstrates the importance of the small features of the landing gear in generating noise, which are the only difference between the two configurations shown in Fig. 15. Note that this is also the most important frequency domain in calculating the noise metric for aircraft noise certification. The impact of these small details on the EPNL calculation will be further discussed later.

To see how the small features affect the source distribution, the measurements from the side-view phased array for the clean configuration are shown in Fig. 16 at four frequencies. The small features are the hydraulic hoses and associated attachments and the brake braces, both located behind the torque link with the former above the latter. Both of them are shown in the photographs in Fig. 5, but are not plotted in the array map in Fig. 16. When Fig. 16 is compared with Fig. 11, which is for the fully dressed gear at the same frequencies, it is clear that the source strength for the clean gear is significantly weaker than the fully dressed gear. This leads to the SPL difference measured by the free-field microphone, shown in Fig. 15. When the difference is taken between the two configurations, the high-frequency noise from the small parts of the gear assembly can be found, which is shown in Fig. 17 for the overhead microphone location.

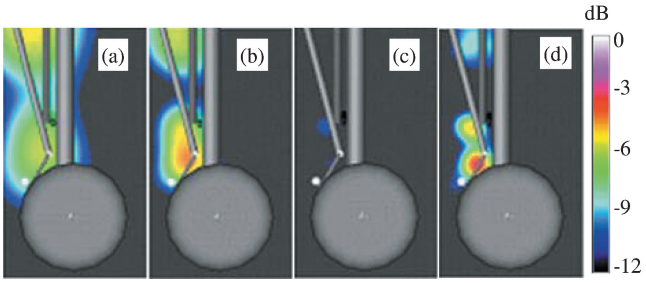

Fig. 16 Phased array measurements from side-view position for clean configuration: a) $f = 1000$ Hz, b) $f = 1500$ Hz, c) $f = 2000$ Hz, and d) $f = 2500$ Hz.

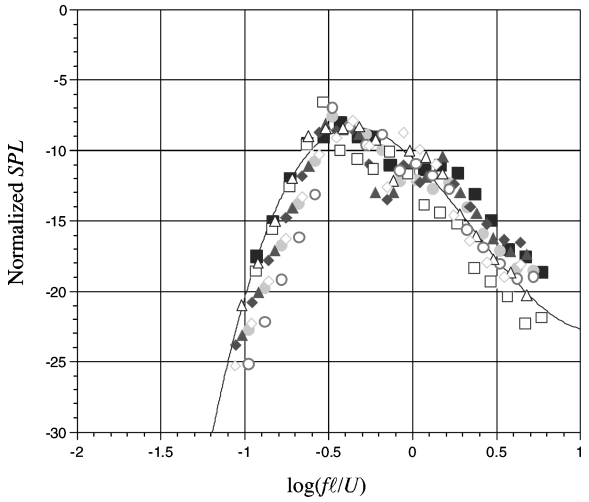

Fig. 17 High-frequency noise due to small details in landing gear assembly at 90-deg emission angle; results are difference between full configuration and clean configuration.

IV. Empirical Prediction

Based on the data analysis described in the preceding section, we developed an empirical prediction scheme, which is given in this section. The development procedure starts with identifying parameters that dominantly control the noise and are covered by the database. Functional dependencies between the radiated noise and these parameters are then derived by a combination of aeroacoustic theory and data analysis using linear regression and correlation analysis. The functional dependencies of the noise on some parameters, such as the flow Mach number, are guided by existing theories of flow noise, such as the acoustic analogy, which, for example, predicts a sixth power law of the body noise dependence on the flow Mach number for low and mid frequencies. The law of spherical spreading of sound waves also easily sets the dependence of the noise on the radial distance to the microphone location. Because the empirical tool is meant to be used for practical predictions, we focused more on the consistency with physics than the last-digit accuracy coming out of the data analysis. A good example of this is again the Mach number scaling. When linear regression is strictly applied to the database, a power law of slightly less than six can be found for the OASPLs. Instead of this, we choose to be consistent with aeroacoustic theories and simply set the power law to six. The difference between the two is insignificant for practical predictions.

The empirical prediction involves the summation of the three spectral components, namely, the low-, mid-, and high-frequency noise. The summation is on the energy basis, neglecting the interferences between the spectral components, which can be written as

$$\langle p^2 \rangle = \langle p_L^2 \rangle + \langle p_M^2 \rangle + \langle p_H^2 \rangle \tag{1}$$

where the subscripts L, M and H indicate the low-, the mid-, and the high-frequency component and the angle brackets mean ensemble average. For each spectral component, the SPL is assumed to be a function in the general form of

$$\text{SPL} = \text{OASPL} + F(Sr) \tag{2}$$

where OASPL is a function defined by

$$\text{OASPL} = \text{OASPL}(M, R, \theta, \ell, N_s, N_w, \eta) \tag{3}$$

and F is the normalized spectrum.

Here the flow is specified by the local flow Mach number M, which should be considered as the flow Mach number upstream of the landing gear. The far-field microphone location is defined by the radial distance R and polar angle θ, which are measured in emission coordinates. No azimuthal angular variation is considered here because landing gear noise is of concern only in the overhead fly-over plane. The landing gear components are characterized by the length scale ℓ and are the diameter of the wheels, the mean value of the cross section dimensions of the main struts, and the typical size of the small parts, respectively, for the three groups of the gear components. Also, we have used N_s and N_w to denote the number of main struts and the number of wheels, respectively, in the gear assembly. To account for the effects of the small details in the landing gear, which can significantly increase the high-frequency noise as revealed in the test data discussed in the preceding section, we have introduced a complexity factor η, and its contribution to the OASPL is also included in result (3). The frequency dependence in Eq. (2) is explicitly accounted for by the function F, which depends only on the Strouhal number Sr, defined by

$$Sr = f\ell/U \tag{4}$$

with f the one-third octave band center frequency and U the local flow velocity. The length scale ℓ should be chosen to be its respective value for each of the three components.

As defined in Eq. (3), the OASPL is computed as a function of flow and geometry parameters associated with a landing gear assembly, as well as the far-field microphone locations. For all three components, the OASPL is expressed by the general form

$$\text{OASPL} = 20\log(\ell/R) + C_0 + C_1\log(M) - C_2\log(\sin\theta) + C_3\log(N_s) + C_4\log(N_w) + C_5\log(\eta) \tag{5}$$

which involves six constants. These are derived by linear regression analysis of the test data for each of the three spectral components. The results are summarized in Table 4. These constants determine the functional dependencies of the overall noise on the geometry and flow conditions and measurement locations. The spherical spreading law is followed by all three components so that we simply assume the same dependence for all three components. The normalized spectrum F in Eq. (2) is given for each of the three frequency components, and all three can be expressed in the general form

$$F(Sr) = \sum_{n=0}^{5} B_n[\log(Sr)]^n \tag{6}$$

where the Strouhal number Sr is defined by Eq. (2) and the six constants B_n, $n = 0, 1, 2, 3, 4$, and 5, are given in Table 5. These

Table 4 Coefficients for OASPL calculation

	Frequency domain		
Coefficients	Low	Mid	High
C_0	145.7	168.5	185.3
C_1	60.0	60.0	70.0
C_2	4.3	2.4	9.0
C_3	0.0	10.0	10.0
C_4	10.0	0.0	0.0
C_5	0.0	0.0	10.0

Table 5 Coefficients for the normalized SPL

	Frequency domain		
Coefficients	Low	Mid	High
B_0	−9.6866	−13.921	−10.892
B_1	1.9071	−5.9695	−9.3852
B_2	−3.7577	−3.6107	9.2856
B_3	0.0	0.6181	0.4813
B_4	0.0	0.0	−2.4532

values are derived by applying linear regression analysis to each of the three frequency components and the rms error of the analysis is respectively 1.168, 0.992, and 1.101 dB for the low-, the mid-, and the high-frequency component.

The Mach number dependence is given in Eq. (5) by the term involving C_1, which, as shown in Table 4, is equal to 60 for the low- and mid-frequency component and 70 for the high-frequency domain, respectively, corresponding to the sixth and seventh power law. The physics of such different scaling laws for the different frequency components is discussed in the preceding section, reflecting the different source behavior. The values are simply derived from the scaling laws without any curve fitting or linear regression analysis. This is justified by the data shown in the preceding section. If linear regression analysis is used to derive the values for C_1, slightly different results may be found. For example, the low- and mid-frequency noise may scale on the Mach number to the power of 5.8 instead of 6. This may be because the length scale of the noise sources is not exactly the physical dimensions of the gear components. They are usually also Mach number dependent. However, this would only result in slight differences in the overall prediction, which for empirical prediction can be considered insignificant. Also note that, though the data analysis in the preceding section shows the nature of the high-frequency noise source to be quadrupolelike, implying an eighth power law for the OASPL, the empirical formula (5) is given by the seventh power on Mach number. There are two reasons for this. One is that the eighth power law is followed if the SPL is integrated in fixed-Strouhal number bands to derive the OASPL, which is usually not the case in practical applications. Instead, practical applications almost always integrate SPL with fixed-frequency bands. Thus, the Mach number scaling should be the same for both SPL and OASPL. The second reason is that the high-frequency spectrum is derived by applying the Mach number scaling (seventh power) to the SPL and then taking the difference between the fully dressed and the clean configuration. When the resulting spectra are used to calculate the OASPL, the Mach number dependence has already factored out of the data sets by the seventh power law. If the differences between the fully dressed and the clean gear were taken for each case of different Mach numbers before the Mach number scaling, the resulting spectra would need to be scaled by the eighth power and so would the OASPL. Because we are mainly interested in empirical prediction here, this detailed data analysis is not followed.

The directivity of the radiated noise is given in Eq. (5) by the term involving C_2. From the values in Table 4, it is clear that the directivities for the three frequency components are similar. This is probably due to the complexity of the sources that have irregular orientations. It can be noted that the directivities of all three components show more noise in the upstream and downstream direction and minimum noise at the overhead location. This has also been observed in previous experimental studies and in the numerical study of Ref. 11 for the low-frequency noise from a simple gear (noise computed in Ref. 6). This is probably because many of the gear components, such as the main struts, are orientated with their longitudinal axes perpendicular to the flow direction, causing more radiation in the upstream and downstream direction than the overhead location.

The effects of the number of wheels and main struts are included in the empirical prediction (5) by simply assuming incoherent energy addition. The limited number of configurations tested clearly does not allow a detailed correlation analysis on the wheel number and strut number. However, as shown in the preceding section, the data seem to follow the simple energy addition quite well, and this is what has been implemented in Eq. (5). Obviously, the number of wheels dominantly affects the low-frequency component, and the number of struts mainly affects the mid- and high-frequency noise.

The last term in Eq. (5) is our attempt to capture the effects of small details in the landing gear assembly and, thus, provide a simple way to predict the high-frequency noise. Note that this term is only based on physical reasoning without data to validate it. It is more a concept that needs further development than a mature prediction tool. It is easy to realize that it is not practical to describe precisely the small parts such as the hydraulic hoses and attachments and the small geometry irregularities such as steps and cutouts for noise prediction. The data analysis given in the preceding section also indicates that such a precise description may not be necessary either. The far-field SPL is shown to follow the seventh power law on Mach number, implying the role of the turbulent wake in generating the high-frequency noise. This is supported by the phased microphone array measurements, which identify the wake as significant sources. Thus, the noise-generation mechanisms may be more similar to turbulent flow noise best described by the statistics of the flow than any deterministic mechanisms. The intensity of the wake, which determines the noise, is of course a function of the small details in the gear that produces the wake. Intuitively, the more complex the gear is, the more intense the wake flow will be. Thus, it is logical to seek a parameter to describe the complexity of the gear, hoping that it can be correlated to the high-frequency noise. This is why we introduced the complexity factor η in the empirical prediction (5). To proceed further, the complexity factor needs to be related to measurable quantities to allow for meaningful noise prediction. As a first cut, we argue that larger airplanes usually need more complex landing gears and, hence, generate more high-frequency noise. Thus, we can assume that the complexity factor is proportional to the maximum gross takeoff (or landing) weight, which is an important parameter in aircraft design. Based on this concept, some examples will be given in the next section.

V. Code Validation and Application

The empirical prediction scheme given in the preceding section is very easy to implement, with only a small group of parameters needed for the noise calculations, the flow Mach number being one of them. It is important to emphasize that the flow Mach number in the prediction scheme is that just upstream of the gear assembly. Because the test data, on which the prediction scheme is based, are for an isolated gear with no installation effects, the Mach number in the database is also the freestream Mach number. When the prediction is applied to aircraft landing gears that are installed, the input Mach number, defined as just upstream of the gear, is very often different from the freestream (or flight) Mach number. For both the main landing gear and the nose gear, the installation effects may noticeably change the local flow. For the main gear, which is located under the wing, the high-lift system slows down the flow under the wing, resulting in a smaller local Mach number than the freestream Mach number. For the nose gear, the local Mach number is higher because the flow is accelerated as it passes along the aircraft nose. To demonstrate the effects of this change of local flow conditions, Fig. 18 shows the flow velocity below the Boeing 737 airplane at 4 deg of angle of attack with flaps deployed at 30 deg, calculated by using a potential flow method. The velocity is normalized by the freestream velocity and is plotted as a function of the distance from the bottom of the aircraft. The location of the gear assembly is also indicated in Fig. 18. As is shown, the velocity at the gear location is only about 80% of the freestream velocity. This variation can lead to significant difference in noise prediction; for example, based on the sixth power law, it corresponds to a difference in noise of about 5.8 dB.

To validate the prediction scheme, predictions were compared extensively with data for the Boeing 737 airplane, showing very good agreement in various flow conditions and measurement locations. This is expected because the prediction formulas were derived

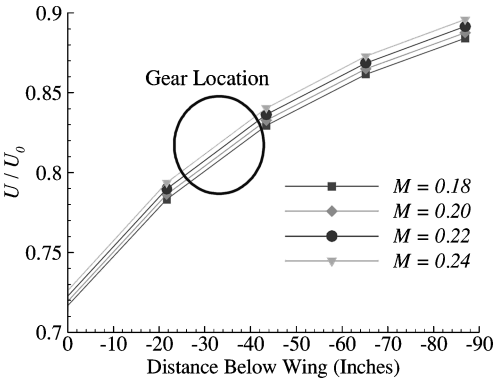

Fig. 18 Mean flow velocity under wing for Boeing 737 aircraft.

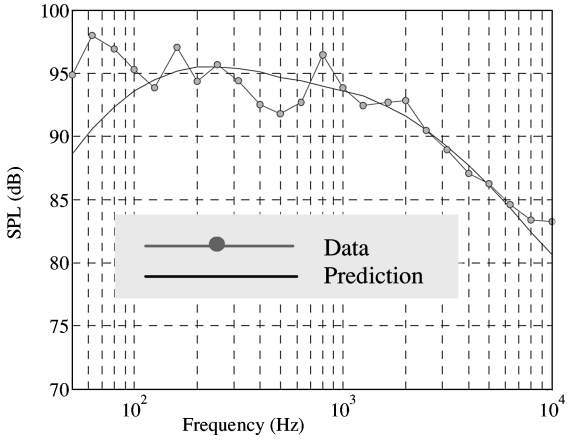

Fig. 19 Spectrum comparison for Boeing 737 landing gear for $M = 0.24$ at the fly-over position: ——, prediction and ○, test data.

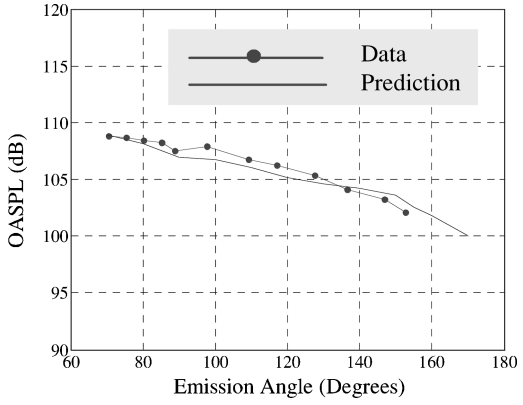

Fig. 20 OASPL for Boeing 737 landing gear at $M = 0.24$: ——, prediction and ○, test data.

from the Boeing 737 database. Thus, only two examples are given here to show the good agreement between the prediction and data in Figs. 19 and 20, respectively, for the case of $M = 0.24$. Figure 19 shows the spectrum at 90-deg emission angle, and Fig. 20 shows the directivity in terms of OASPL. For both, the comparison with data is very favorable. To further demonstrate the application of the empirical prediction, estimates are made and shown in Figs. 21–23 for a few Boeing airplanes at a Mach number of 0.18. Figure 21 shows the noise spectra at 90 deg of emission angle, with a progressive noise increase from small to large airplanes. The same trend is also shown in Fig. 22 for the OASPL on a 10-ft arc and in Fig. 23 for the EPNL. Though no absolute levels are given and no data comparison is presented here, the trend appears to be consistent with measurements.

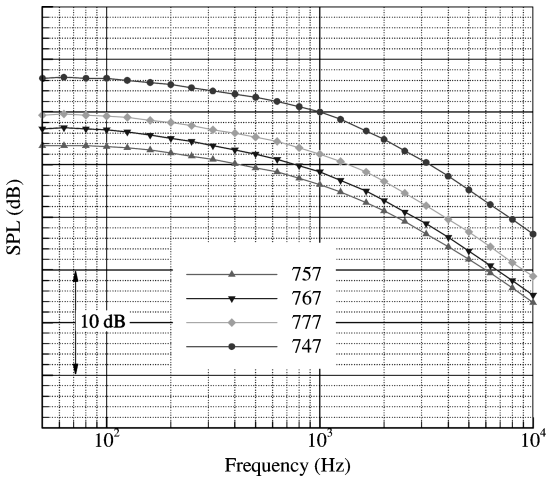

Fig. 21 Prediction of landing gear noise spectrum for various aircraft types for $M = 0.18$ at 90-deg emission angle.

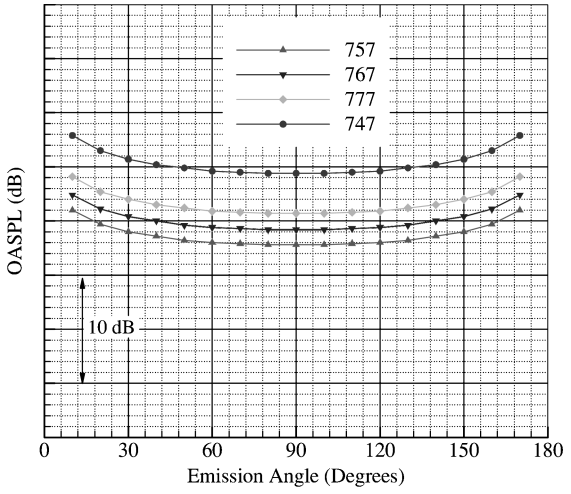

Fig. 22 Prediction of landing gear noise directivity for various aircraft types for $M = 0.18$ on 10-ft arc.

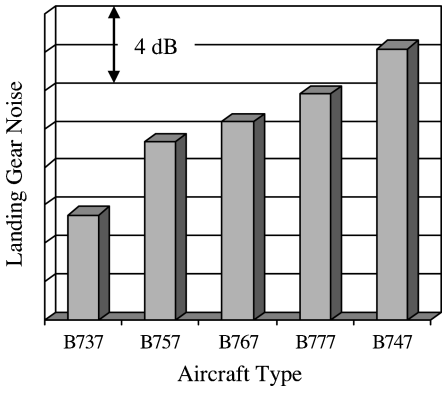

Fig. 23 Total landing gear noise (EPNL) prediction for various aircraft types.

To see how the present prediction scheme compares with other models, a comparison study was done with Fink's airframe noise prediction code, which has been widely used in the past.[1,2] The two approaches were used to predict the same Boeing 737 landing gear. For the three frequency domains, the length scales were chosen to be the wheel diameter (50 in.), the mean strut diameter (5 in.), and the typical hydraulic pipe diameter (0.5 in.). The local flow Mach number was determined as 83% of the flight Mach number based on the potential flow code output. Because the empirical scheme

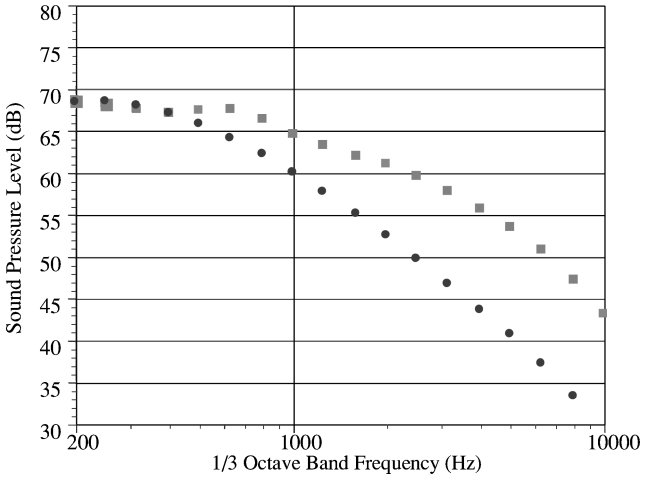

Fig. 24 Spectrum comparison for emission angle of 90 deg: ○, Fink's method and □, present model.

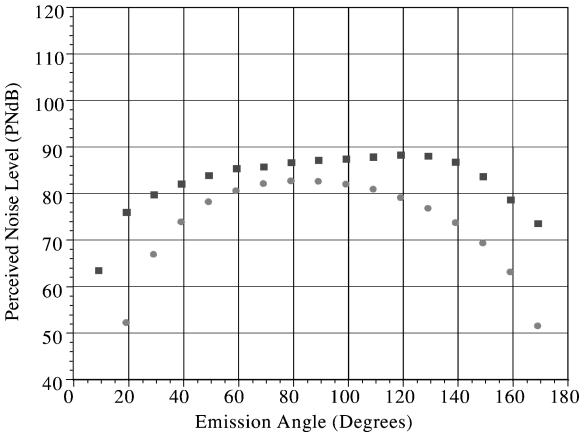

Fig. 25 Directivity comparison between along a line in fly-over plane: ○, Fink's method and □, present model.

is based on the Boeing 737 data, this aircraft configuration can be taken as the baseline and the complexity factor can be set to one for this case.

The predicted spectra from the two methods are compared in Fig. 24 for the overhead location at $M = 0.24$. As is clear from Fig. 24, the two predictions agree with each other reasonably well at low frequencies, but Fink's code shows a faster rolloff in the high-frequency region, leading to significant underprediction. Fink's model does not explicitly address high-frequency noise. This high frequency discrepancy is due to the fact that Fink's landing gear noise prediction was developed from simple small-scale landing gear models that lacked small features responsible for the high-frequency noise generation. This is actually a lesson learned in recent years in landing gear noise research; studies based on small-scale models that are inevitably simplified are likely to miss the important high-frequency noise and any landing gear noise prediction tools developed based on simplified small-scale models are likely to underpredict the high-frequency noise. To see the impact of this underprediction on practical noise metrics such as the EPNL, the noise levels used to calculate EPNL are shown in Fig. 25, together with the values of the EPNL, showing the significant underprediction of the Fink's model with a discrepancy in EPNL as much as 8 dB.

VI. Conclusions

We have presented an experimental study on aircraft landing gear noise, including the tests, the data analysis, and the development of an empirical prediction scheme. By testing a series of gear configurations with various degree of complexity, we have explicitly revealed contributions of different gear components to the total landing gear noise. The landing gear assembly has been cataloged into three groups, namely, the wheels, the main struts, and the small details, which generate noise in the low-, the mid-, and the high-frequency domain, respectively. Parametric trends have been identified for each of the three spectral components in terms of the flow Mach number, gear geometry parameters, and microphone locations. This not only provides a full-scale test database for developing prediction tools, but also sheds new light on the source mechanisms, which can help both tool development and noise reduction concept design. By combining free-field microphone data with phased microphone array measurements, we have shown that the turbulent wake of the gear assembly plays an important role in generating the high-frequency noise; the phased array identifies a distribution of sources in the wake region at high frequencies, and the high-frequency noise measurements from the far-field microphones has spectral shapes and Mach number scaling typical of turbulence-generated noise. At low and mid frequencies, our experimental study confirms the sixth power law scaling on the flow Mach number, attributing the noise to the unsteady forces on the surfaces of the gear parts. Our data analysis has also revealed the effects of the gear geometry parameters. For noise in the low- and mid-frequency domain, noise from individual wheels and struts follows incoherent energy addition; the total noise is proportional to the number of gear components. At high frequencies, the counting of small parts and small geometry features, which are responsible for the high-frequency noise generation, becomes impractical. Thus, we have proposed to use a complexity factor to account for the aggregate effects. We have also discussed ways to link this complexity factor to measurable parameters in aircraft design so that practical noise prediction become feasible. An empirical prediction scheme has been presented, and some examples of practical applications have been given, that show consistent trends with data.

Acknowledgments

A large part of the database used in this paper was collected under the NASA Advanced Subsonic Technology Program, and the development of the empirical model was partially funded by NASA with R. A. Golub as Technical Monitor. The authors wish to thank R. A. Golub for his support.

References

[1]Fink, M. R., "Airframe Noise Prediction Method," Federal Aviation Administration, Rept. FAA-RD-77-29, 1979.

[2]Fink, M. R., "Noise Component Method for Airframe Noise," *Journal of Aircraft*, Vol. 16, No. 10, 1979, pp. 659–665.

[3]Heller, H., and Dobrzynski, W., "Sound Radiation from Aircraft Wheel-Well/Landing-Gear Configuration," *Journal of Aircraft*, Vol. 14, No. 8, 1977, pp. 768–774.

[4]Smith, M. G., and Chow, L. C., "Prediction Method for Aerodynamic Noise from Aircraft Landing Gear," AIAA Paper 98-2228, June 1998.

[5]Smith, M. G., and Chow, L. C., "Validation of a Prediction Model for Aerodynamic Noise from Aircraft Landing Gear," AIAA Paper 2002-2581, June 2002.

[6]Guo, Y. P., "A Statistical Model for Landing Gear Noise Prediction," *Journal of Sound and Vibration*, Vol. 282, No. 1–2, 2005, pp. 61–87.

[7]Dobrzynski, W., and Buchholz, H., "Full-Scale Noise Testing on Airbus Landing Gears in the German Dutch Wind Tunnel," AIAA Paper 97-1597, May 1997.

[8]Stoker, R. W., "Landing Gear Noise Test Report," NASA Contract NAS1-97040, Aug. 1997.

[9]Jaeger, S. M., Burnside, N. J., Soderman, P. T., Horne, W. C., and James, K. D., "Microphone Array Assessment of an Isolated 26%-Scale High Fidelity Landing Gear," AIAA Paper 2002-2410, June 2002.

[10]Dobrynski, W., Chow, L. C., Guion, P., and Shiells, D., "Research into Landing Gear Airframe Noise Reduction," AIAA Paper 2002-2409, June 2002.

[11]Hedges, L. S., Travin, A., and Spalart, P. R., "Detached-Eddy Simulations over a Simplified Landing Gear," *Journal of Fluids Engineering*, Vol. 124, No. 2, 2002, pp. 413–423.

[12]Li, F., Khorrami, M. R., and Malik, M. R., "Unsteady Simulation of a Landing Gear Flow Field," AIAA Paper 2002-2411, June 2002.

[13]Souliez, F. J., Long, L. N., Morris, P. J., and Sharma, A., "Landing Gear Aerodynamic Noise Prediction Using Unstructured Grids," AIAA Paper 2002-0799, June 2002.

[14]Ffowcs Williams, J. E., "Hydrodynamic Noise," *Annual Review of Fluid Mechanics*, Vol. 1, 1969, pp. 197–222.

[15]Crighton, D. G., "Basic Principles of Aerodynamic Noise Generation," *Progress in Aerospace Sciences*, Vol. 16, No. 1, 1975, pp. 31–96.

[16]Crighton, D. G., "Airframe Noise," *Aeroacoustics of Flight Vehicles: Theory and Practice*, NASA RP-1258, Vol. 1, 1991, pp. 391–447.

[17]Lighthill, M. J., "On Sound Generated Aerodynamically I. General Theory," *Proceedings of the Royal Society of London, Series A: Mathematical and Physical Sciences*, Vol. A 211, 1952, pp. 564–587.

[18]Ffowcs Williams, J. E., "Sound Radiation from Turbulent Boundary Layers Formed on Compliant Surfaces," *Journal of Fluid Mechanics*, Vol. 22, No. 2, 1965, pp. 347–358.

[19]Amiet, R. K., "Refraction of Sound by a Shear Layer," *Journal of Sound and Vibration*, Vol. 58, No. 4, 1978, pp. 467–482.